Catalytic enhancement on Ti-Zr complex oxide particles for electrochemical hydrogenation of oxalic acid to produce an alcoholic compound by controlling electronic states and oxide structures

SCHOLARONE™
Manuscripts

Journal Name

COMMUNICATION

Catalytic enhancement on Ti-Zr complex oxide particles for electrochemical hydrogenation of oxalic acid to produce an alcoholic compound by controlling electronic states and structures†

M. Yamauchi,[a]* S. Hata,[b] H. Eguchi,[c] S. Kitano,[a] T. Fukushima,[a] M. Higashi,[a] M. Sadakiyo,[a] K. Kato[d]*

$Ti_{1-x}Zr_xO_2$ complex oxide particles with $0.02 \leq x \leq 0.1$ show superior catalytic performances for the direct power storage into glycolic acid via electroreduction of oxalic acid. The atomic pair distribution function analysis of X-ray total scatterings suggested that structural periodicity is the key factor for the catalytic enhancement.

The electrochemical reduction using water as a hydrogen source realizes direct electric power storage in high-energy chemicals or fuels with a minimum environmental load.[1] Liquid chemicals that are electrochemically produced from CO_2, such as formic acid[2] and alcohols,[3] have attracted significant attention in terms of carbon-neutrality, storability and transportability, although CO_2 capture is another challenge.[4] The electrochemical reduction of bio-derivable and water-soluble organic acids can be a profitable route for preparing low-carbon alcohols.[5] However, a chemically stable carboxylic acid is commonly converted under severe conditions by using H_2 gas directly [6-7] or indirectly.[8] In contrast, the electrochemical hydrogenation of oxalic acid (divalent carboxylic acid, HOOC-COOH, OX) is achievable using anatase TiO_2 catalysts under mild conditions.[9] In this system, glycolic acid (HOOC-CH_2OH, GC), a corresponding alcoholic derivative, is produced via the 4-electron reduction of OX, which affords efficient electronic power storage into GC with a high volumetric energy density, 8,600 MJm^{-3}, cf., 13 MJm^{-3} for H_2 gas.[9] GC is available for a broad range of applications[10,11] due to its superior solubility, chemical stability, and low corrosivity; i.e., industrially available GC can be synthesized by using renewable electricity. Noted that the electroreduction of OX on a ubiquitous TiO_2 catalyst proceeds selectively (>98% selectivity) in an acidic aqueous solution

(pH=2.1), where H_2 evolution is expected to be highly preferable.[12]

TiO_2 has been intensively investigated as a benchmark oxide catalyst because of its superior photocatalytic performances. Significant efforts have been devoted to enhancing the catalytic activities of TiO_2 by creating favorable surface structures,[13] the band gap energy (E_g)[14] and impurity levels.[15] To further improve electrocatalytic activities of TiO_2 catalysts for OX reduction, we focus on partial substitution of Ti ions with Zr ions in the oxide catalyst. A Zr ion is characterized by a valence state similar to that of a Ti ion but a larger ionic radius than that of Ti ion; e.g, the ionic radii of Zr^{4+} and Ti^{4+} ions are 0.720 and 0.605 Å, respectively, which is suitable for a dopant for a slight modification of electronic and geometric structures of TiO_2. Ti-ZrO_2 complex oxides have already been found to show catalytic performance superior to those observed on pure TiO_2 due to the increase in surface area,[16] enhancement of electron transfer,[17] and emergence of surface acidity.[16, 18] Herein, we first utilized Ti-ZrO_2 particles for the electroreduction of an organic acid and found that a small amount of Zr inclusion modifies both crystal structure and electronic states of TiO_2 particles, which significantly improves the catalytic activities for the OX electroreduction. Detailed structural characterization of Ti-ZrO_2 particles using the atomic pair distribution function (PDF) analysis of synchrotron X-ray total scattering (SXTS) uncovered that the periodicity of atomic positions is more important than

a. *International Institute for Carbon-Neutral Energy Research (WPI-I2CNER), Kyushu University, Motooka 744, Nishi-ku, Fukuoka 819-0395, Japan.*
b. *Department of Applied Chemistry, Faculty of Engineering, Sanyo-Onoda City University, Daigakudo-ri, 1-1-1, Sanyo-Onoda, Yamaguchi 756-0884, Japan.*
c. *Department of Chemistry, Graduate School of Science, Kyushu University, Motooka 744, Nishi-ku, Fukuoka 819-0395, Japan.*
d. *RIKEN SPring-8 Center, 1-1-1 Kouto, Sayo-cho, Sayo-gun, Hyogo 679-5148, Japan.*
†Electronic Supplementary Information (ESI) available: Experimental details, SEM, SEM-EDS, TEM, PXRD, N_2 adsorption-desorption isotherms, CV and PDF data. See DOI: 10.1039/x0xx00000x

Figure 1. SEM (upper) and TEM (lower) images for (a, e) TiO_2, (b, f) $Ti_{0.9}Zr_{0.1}O_2$, (c, g) $Ti_{0.75}Zr_{0.25}O_2$, (d, h) ZrO_2

are the bond length and crystallinity (crystallite size) for the electrochemical hydrogenation of OX.

We prepared Ti-ZrO$_2$ complex oxide particles with an entire range of composition via a solvothermal method, i.e., the reaction of titanium tetraisopropoxide and zirconium propoxide in acetone under solvothermal conditions, which enables the preparation of Ti-ZrO$_2$ particles that are homogeneous in shape.[19, 20] The detailed synthetic procedure is provided in Electronic Supplemental Information (ESI). The morphology and size distribution of the prepared samples were examined via scanning electron microscopy (SEM) and transmission electron microscopy (TEM) measurements. Figures 1a-d and S1-11 show that all prepared samples include spherical particles with average diameters of 2-5.5 μm (Figure S12). The elemental compositions determined by the energy dispersive X-ray spectroscopy (EDS) measurements agree well with a starting composition ratio (Table S1, Figure S13). Thus, we specify the complex oxide using the starting Zr content (x) as Ti$_{1-x}$Zr$_x$O$_2$. The EDS signals of Ti-K and Zr-L were distributed over the particle with x≥0.1 (Figures S5-11), indicating that Zr ions are homogeneously dissolved in the particle, whereas the Zr signals from the samples with x≤0.005 were too weak for visualization. From TEM observations, we found that oxide spheres are composed of small crystal grains, the size of which increases with an increase in the Zr content to x=0.15 but decreases in Zr-content range from x=0.2 to 0.5. Interestingly, Ti$_{0.25}$Zr$_{0.75}$O$_2$ and ZrO$_2$ particles have a smooth surface, implying these particles are composed of
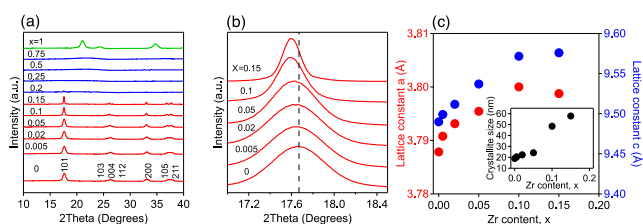
Figure 2. (a) XRD patterns of Ti$_{1-x}$Zr$_x$O$_2$ particles and (b) extended patters of (a). (c) Lattice constants of anatase Ti$_{1-x}$Zr$_x$O$_2$ particles. Crystallite sizes of Ti$_{1-x}$Zr$_x$O$_2$ particles determined via Rietveld analyses are shown in the inset.

larger crystallites (Figures 1e-h, S1-11).

The X-ray diffraction (XRD) pattern of the TiO$_2$ particle shown in Figure 2a can be attributed to an anatase-type TiO$_2$ phase. Ti$_{1-x}$Zr$_x$O$_2$ particles, which included a small amount less than 15 atom% of Zr exhibited XRD patterns analogous to the pattern observed for TiO$_2$ particles (Figures S14-19), although very small peaks from the brookite phase were observed for the Ti$_{0.9}$Zr$_{0.1}$O$_2$ and Ti$_{0.85}$Zr$_{0.15}$O$_2$ particles (Figures S18 and 19). However, Ti$_{1-x}$Zr$_x$O$_2$ particles with x=0.2-0.75 showed no obvious diffraction peaks, indicating that these complex oxide particles have no crystalline phase but an amorphous phase, as previously reported (Figure 2a).[20] The XRD pattern of ZrO$_2$ particle corresponds to the pattern of a pure tetragonal phase of ZrO$_2$ (Figure 2a). Expanded 101 diffraction peaks observed for Ti$_{1-x}$Zr$_x$O$_2$ with x≤0.15 are provided in Figure 2b. The peak positions were gradually shifted to the lower angle side with an increase in Zr content up to x=0.1. Structural parameters, which were determined via the Rietveld analysis of XRD patterns, are summarized in Table S2. The lattice constants a and c of an anatase phase were gradually increased with the Zr content, as confirmed by the peak shifts toward the lower angle side to x=0.1 (Figures 2b and 2c). The increase of lattice constants can

be attributed to substitution of a Zr ion for a Ti site. Thus, we conclude that solid solutions of Ti$_{1-x}$Zr$_x$O$_2$ particles with an anatase structure are formed in the composition region of x=0.005-0.1. At x=0.15, the complex oxide exhibited smaller a and larger c values than did those for the oxides with x≤0.1. This irregular behavior possibly implies that Ti$_{0.85}$Zr$_{0.15}$O$_2$ particles are near the critical state between anatase and amorphous phases but still contain an anatase one. Noted that the peak widths for Ti$_{0.9}$Zr$_{0.1}$O$_2$ and Ti$_{0.85}$Zr$_{0.15}$O$_2$ particles were narrowed with Zr content compared with that for the TiO$_2$ ones, which is consistent with increase in the crystallite size with Zr content to 0.15 (inset of Figure 2c). These results suggest that solidification of certain amount of Zr ions improves the crystallinity of anatase phases. The surface area determined from the nitrogen adsorption isotherms increased from 98 to 387 m^2 g^{-1} according to the increase of Zr content from x=0.1 to 0.5 and decreased above x=0.5, which revealed that anatase particles do not possess larger surface areas compared with amorphous particles (Figures S20 and S21a). Pore volumes of the catalysts were obtained from N$_2$ adsorption and were found to reach the maximum at x=0.2 (Figure S21b).

We examined the electronic structures of the prepared catalysts. Figure S22 shows the UV-vis diffuse reflectance spectra for Ti-ZrO$_2$ particles. Ti-ZrO$_2$ particles exhibited a blue-shifted spectrum compared with that for pure TiO$_2$, which is attributable to the changes in E_g values due to the incorporation of Zr ions into the TiO$_2$ lattice. Figure 3a presents E_g values calculated from UV-vis spectra. The E_g values for anatase Ti$_{1-x}$Zr$_x$O$_2$ particles with x=0.005-0.1, i.e., 3.35-3.38 eV, were greater than 3.28 eV for TiO$_2$ particles, but these values did not drastically change in this composition region. At x≥0.2, the E_g values proportionally increased with Zr content, i.e., 3.35-4.13 eV, similar to the trends observed in previous reports.[17, 21, 22] We measured electric conductivities of some representative catalysts and found that the conductivity of Ti$_{0.995}$Zr$_{0.005}$O$_2$, Ti$_{0.95}$Zr$_{0.05}$O$_2$, Ti$_{0.75}$Zr$_{0.25}$O$_2$ and Ti$_{0.75}$Zr$_{0.25}$O$_2$ at 323 K are 3.86•10^{-9}, 1.65•10^{-9}, 6.6•10^{-10} and 8.4•10^{-9} Scm^{-2}, respectively. This result suggests that the conductivity does not simply follow the Zr content but is related with E_g values and the grain size of the catalyst. Figure 3b describes energy levels of the valence band maximum (VBM) and the conduction band bottom (CBB) from vacuum level, which were calculated using ionization energies obtained from ultraviolet photoelectron spectra of Ti$_{1-x}$Zr$_x$O$_2$ particles with x=0, 0.005, 0.1, 0.15, 0.5 (Figure S23) and E_g (see ESI). Surprisingly, adding a small amount of Zr ions drastically changed the energy states of the Ti-ZrO$_2$ particles, i.e., the CBB energy of Ti$_{0.995}$Zr$_{0.005}$O$_2$ particles, -3.0 eV, is much higher than -4.7 eV of
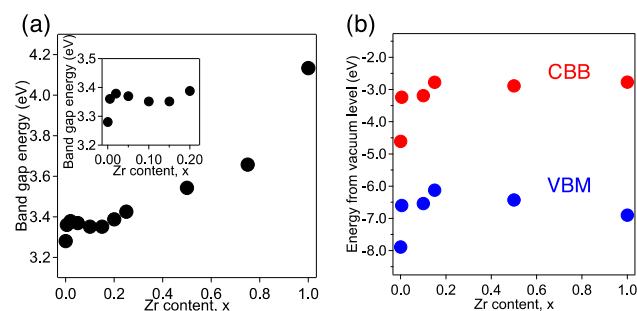
Figure 3. (a) Band gap energy (E_g) and (b) energy levels of valence band maximum (VBM) and conduction band bottom (CBB) of Ti$_{1-x}$Zr$_x$O$_2$ particles. E_g values of Ti$_{1-x}$Zr$_x$O$_2$ particles with x≤0.2 are shown in inset.

TiO_2 particles, which implies that CBB levels were shifted to the higher energy level toward the vacuum level. When electric potential is applied to a circuit, electrons are introduced into vacant levels in the CBB of cathode catalysts. Electrons, which are placed at higher CBB levels, possibly have a higher reducing ability.[9] However, amorphous $Ti_{1-x}Zr_xO_2$ particles, which are characterized by higher CBB levels, showed a considerably lower selectivity for the OX reduction compared with pure TiO_2 and anatase $Ti-ZrO_2$ particles. Therefore, a higher CBB level does not seem to be a prerequisite for efficient OX reduction on $Ti-ZrO_2$ particles.

Valence states and surface distributions of constituent ions were examined using X-ray photoelectron spectroscopy (XPS) measurements, as shown in Figures S24 and S25. For all samples, two kinds of peaks for Ti and O species were observed. XPS signals observed at 458.5 and 456.7 eV can be attributed to Ti^{4+} in a lattice and Ti^{3+} at surface defects, and those at 531.2 eV and 529.7 eV were attributed to an oxygen in a lattice and an oxygen of a surface hydroxyl group, respectively.[23, 24] Signals observed at 181.8 eV for $Ti_xZr_{1-x}O_2$ particles with x≥0.005 can be assigned to a Zr^{4+} specie.[25, 26] Surface concentrations of Ti, Zr, and O ions on the surface agree well with the starting composition although there are no apparent relationship between the composition dependence and catalytic performances. Surface concentrations of Ti species were shown in Figure S26d. The percentage of Ti^{4+} species was monotonically decreased with the Zr content. The percentage of Ti^{3+} ions reached the minimum around x=0.1 and monotonically decreased at x≥0.2, i.e., in the amorphous region. The Ti^{3+} concentration reflects formation of oxygen defects on the surface of anatase TiO_2.[27] Thus, the decrease of the Ti^{3+} concentration from x=0 to x=0.1 implies decrease of surface defects and improvement of crystallinity, which is consistent with the result from XRD measurements as discussed above. Therefore, we can conclude that inclusion of Zr ions contributes to enhancement of crystallinitiy of anantaze $Ti-ZrO_2$ particles.

Catalytic activities of $Ti-ZrO_2$ particles for OX reduction were firstly examined via cyclic voltammetry (CV) measurements at 50 °C, which was the optimized temperature in the previous study.[9] Theoretical electrode potentials are shown below.

Cathode: $HOOC-COOH + 4H^+ + 4e^- \rightarrow$
           $HOOC-CH_2OH + H_2O$ +0.13 V vs RHE.
Anode: $2H_2O \rightarrow 4H^+ + 4e^- + O_2$ +1.23 V vs RHE.
Overall: $HOOC-COOH + H_2O \rightarrow$
           $HOOC-CH_2OH + O_2$ 1.1 V
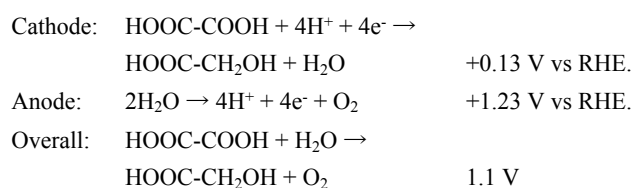
The CV curves without iR corrections shown in Figure S26 reveals that the onset potentials for OX reduction on anatase Ti_{1-}
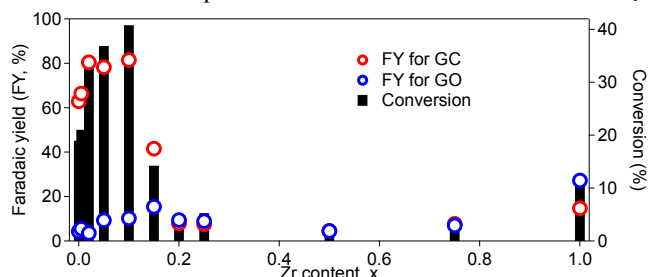
Figure 4. Faradaic yields for GC and GO productions and conversion of OX in electrochemical reduction of OX on $Ti_{1-x}Zr_xO_2$ particles at -0.7 V vs. RHE at 50 °C for 2 h.

$_xZr_xO_2$ particles (x≤0.15) are in the range from -0.03 to -0.20 V vs. RHE, which are more positive than those observed on amorphous type particles, i.e., -0.17 - -0.24 V vs. RHE. Accordingly, the overpotentials were conspicuously changed at the structural transition from an anatase to amorphous phase. Next, we conducted chronoamperometry (CA) measurements on $Ti_{1-x}Zr_xO_2$ particles. Figure 4 indicates conversion of OX and Faradaic yields (FYs) for GC and glyoxylic acid (GO), which is a product via two-electron reduction of OX, in the electrochemical reduction of OX on $Ti_{1-x}Zr_xO_2$ particles at -0.7 V vs. RHE and 50 °C for 2 h. At 0.02≤x≤0.1, the relatively higher FYs for the GC production were achieved, i.e., approximately 80%. Both the conversion of OX and the total yield for productions of GC and GO were maximized on $Ti_{0.9}Zr_{0.1}O_2$ particles, i.e., 40.8 and 91.7%, respectively. These observations imply that anatase $Ti-ZrO_2$ particles, which include 10atom% of Zr ions, efficiently work as a catalyst for the electrochemical reduction of OX compared with pure TiO_2. Amorphous $Ti_{1-x}Zr_xO_2$ particles with x≥0.2, even with a larger surface area up to x=0.5, showed a significantly low catalytic performance compared with anatase particles, which suggests that amorphous structures are not favorable for the OX reduction. Interestingly, pure ZrO_2 particles exhibit a larger FY value than do amorphous ones, implying that crystal formation is more significant. Noted that both surface area and pore volume become the maximum at x=0.5 and 0.2, respectively, whereas the highest OX conversion was observed at x=0.1, which indicates that the surface porosities are not strongly related to the catalytic performance on the complex oxide catalysts. Although binding energies for Ti, Zr and O species changes as a function of the composition range (Figures S25a-c), we could not see any apparent relationships between catalytic performances and changes in the binding energies. These observations clearly suggest that structural factors are more responsible than valence states for achieving notable catalytic activities.

Figure S27a shows the PDF for $Ti_{1-x}Zr_xO_2$ particles with x=0.1 compared with those for x=0 and 1, focusing on shorter distances (r) up to 10 Å. The PDF profile for x=0.1 was in agreement with that for x=0, unlike that for x=1, thus confirming the anatase-type structure. The x=0.15 profile appeared to be similar to that of x=0 but broader than that of x=0, as shown in Figure S27b, suggesting that atomic disordering occurs. However, the x=0.2 profile in Figure S27c was significantly broad, and the intensity was approaching zero at a distance of 10 Å, indicating no long-range order, i.e., a non-crystalline state, as expected. Figures 5a and 5b show average Ti(Zr)-O distances and the distribution of Ti(Zr)-O distances, which were obtained from the position and the width of the PDF peak around 2 Å, respectively, with the FY for GC production. The PDF peak involves both shorter in-plane and longer out-of-plane Ti(Zr)-O
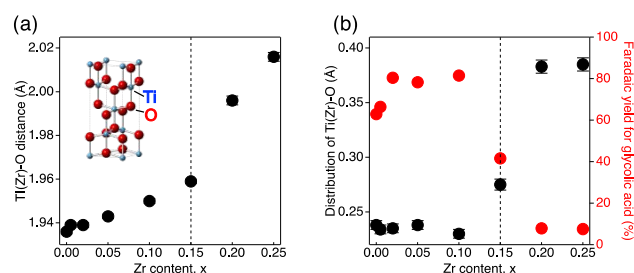
Figure 5. (a) Average bond distance between Ti(Zr) and O (Ti(Zr)-O distance) and (b) the distribution of Ti(Zr)-O distances and the Faradaic yield (FY) for GC production as a function of Zr content, x. Dotted lines indicate a boundary between anatase and amorphous phases.

distances. With an increase in the Zr content, the Ti(Zr)-O distance proportionally increases (Figure 5a), which is related to the increase of E_g values.[22] In contrast, up to x=0.15, the distribution of the Ti(Zr)-O distance is almost constant at the lowest level and the FY for GC production remains constant at the highest level, which suggests that the catalytic performance is associated with degree of ordering in the Ti crystallographic site or the periodicity of atomic positions. Recently, the structural ordering of metal nanoparticles has been focused on as an origin for thermal catalytic reactions.[28] Assuming that the periodicity affects surface and electronic structures,[29] degree of periodicity, that is possibly involved with molecular adsorption,[30] energy-level alignment,[31] etc., becomes significant for the OX electroreduction.

We succeeded in the highly effective electrocatalytic hydrogenation of OX into GC on Ti-ZrO$_2$ particles. The catalytic activity is considerably improved by incorporating Zr ions ≤10 atom% into anatase TiO$_2$ particles, which feasibly relocates the CBB levels of complex oxides higher compared with that of anatase TiO$_2$. Interestingly, the reaction rate obtained using Ti$_{0.9}$Zr$_{0.1}$O$_2$ in this work is considerably high compared to those in our previous work and in the references as shown in Table S3. Detailed structural analysis employing a PDF technique revealed that the periodicity of atomic positions in the oxide crystal is more significant for the electroreduction of OX on oxide catalysts. Metal nanoparticles have been commonly used as an electrocatalysts because of their high conductivity. The findings in this study open the possibilities for the development of highly selective and efficient electrocatalysts composed of oxides via appropriate optimizations of structure and electronic states.

Conflicts of interest

There are no conflicts to declare.

Acknowledgement

References

(1) Kondratenko, E. V.; Mul, G.; Baltrusaitis, J.; Larrazábal, G. O.; Pérez-Ramírez, J. *Energy Environ. Sci.* **2013**, *6*, 3112-3135.
(2) Bai, X.; Chen, W.; Zhao, C.; Li, S.; Song, Y.; Ge, R.; Wei, W.; Sun, Y. *Angew. Chem.* **2017**, *129*, 1-6.
(3) Ma, S.; Sadakiyo, M.; Heima, M.; Luo, R.; Haasch, R. T.; Gold, J. I.; Yamauchi, M.; Kenis, P. J. A. *J. Am. Chem. Soc.* **2016**, *139*, 47-50.
(4) Rochelle, G. T. *Science* **2009**, *325*, 1652-1654.
(5) Naruto, M.; Saito, S. *Nat. Commun.* **2015**, *6*, 8140.
(6) Dub, P. A.; Ikariya, T. *ACS Catal.* **2012**, *2*, 1718-1741.
(7) Manyar, H. G.; Paun, C.; Pilus, R.; Rooney, D. W.; Thompson, J. M.; Hardacre, C. *Chem. Commun.* **2010**, *46*, 6279-6281.
(8) Nystrom, R. F.; Brown, W. G. *J. Am. Chem. Soc.* **1947**, *69*, 2548-2549.
(9) Watanabe, R.; Yamauchi, M.; Sadakiyo, M.; Abe, R.; Takeguchi, T. *Energy Environ. Sci.* **2015**, *8*, 1456-1462, Sadakiyo, M.; Hata, S.; Cui, X. D.; Yamauchi, M. *Sci. Rep.* **2017**, 7, 17032; Sadakiyo, M.; Hata, S.;

Fukushima, T.; Juhász, G.; Yamauchi, M. *Phys. Chem. Chem. Phys.* **2019**, 21, 5882-5889, Fukushima, T.; Higashi, M; Kitano, S.; Sugiyama, T; Yamauchi, M. *Cat. Today* **2019**, in press.
(10) Yamamoto, Y.; Uede, K.; Yonei, N.; Kishioka, A.; Ohtani, T.; Furukawa, F. *J. Dermatol.* **2006**, *33*, 16-22.
(11) Tsai, T.-H.; Wu, Y.-F.; Yen, S.-C. *Microelec. Eng.* **2005**, *77*, 193-203.
(12) Wang, J.; Xu, F.; Jin, H.; Chen, Y.; Wang, Y. *Adv. Mater.* **2017**, *29*, 1605838.
(13) Pan, J.; Liu, G.; Lu, G. Q. M.; Cheng, H. M. *Angew. Chem. Int. Ed.* **2011**, *50*, 2133-2137.
(14) Umebayashi, T.; Yamaki, T.; Itoh, H.; Asai, K. *Appl. Phys. Lett.* **2002**, *81*, 454-456.
(15) Wang, J.; Tafen, D. N.; Lewis, J. P.; Hong, Z.; Manivannan, A.; Zhi, M.; Li, M.; Wu, N. *J. Am. Chem. Soc.* **2009**, *131*, 12290-12297.
(16) Fu, X.; Clark, L. A.; Yang, Q.; Anderson, M. A. *Environ. Sci. Technol.* **1996**, *30*, 647-653.
(17) Neppolian, B.; Wang, Q.; Yamashita, H.; Choi, H. *Appl. Catal. A: Gen.* **2007**, *333*, 264-271.
(18) Tanabe, K.; Sumiyoshi, T.; Shibata, K.; Kiyoura, T.; Kitagawa J. *Bull. Chem. Soc. Jpn.* **1974**, *47*, 1064-1066.
(19) Liu, B.; Liu, L.-M.; Lang, X.-F.; Wang, H.-Y.; Lou, X. W. D.; Aydil, E. S. *Energy Environ. Sci.* **2014**, *7*, 2592-2597.
(20) Uchiyama, H.; Matsumoto, K.; Kozuka, H. *J. Cryst. Growth* **2012**, *338*, 201-207.
(21) Mieritz, D. G.; Renaud, A. l.; Seo, D.-K. *Inorg. Chem.* **2016**, *55*, 6574-6585.
(22) Polliotto, V.; Albanese, E.; Livraghi, S.; Indyka, P.; Sojka, Z.; Pacchioni, G.; Giamello, E. *J. Phys. Chem. C* **2017**, *121*, 5487-5497.
(23) Jensen, H.; Soloviev, A.; Li, Z.; Søgaard, E. G. *Appl. Surf. Sci.* **2005**, *246*, 239-249.
(24) Kumar, P. M.; Badrinarayanan, S.; Sastry, M. *Thin Solid Films* **2000**, *358*, 122-130.
(25) Mahmood, Q.; Afzal, A.; Siddiqi, H. M.; Habib, A. *J. Sol-Gel Sci. Technol.* **2013**, *67*, 670-674.
(26) Tsunekawa, S.; Asami, K.; Ito, S.; Yashima, M.; Sugimoto, T. *Appl. Surf. Sci.* **2005**, *252*, 1651-1656.
(27) Ikeda, S.; Sugiyama, N.; Murakami, S.-y.; Kominami, H.; Kera, Y.; Noguchi, H.; Uosaki, K.; Torimoto, T.; Ohtani, B. *Phys. Chem. Chem. Phys.* **2003**, *5*, 778-783.
(28) Kumara, L. S. R.; Sakata, O.; Kohara, S.; Yang, A.; Song, C.; Kusada, K.; Kobayashi, H.; Kitagawa, H. *Phys. Chem. Chem. Phys.* **2016**, *18*, 30622-30629.
(29) Lu, Z. W.; Wei, S. H.; Zunger, A. *Phys. Rev. B* **1992**, *45*, 10314.
(30) Vittadini, A.; Selloni, A.; Rotzinger, F. P.; Grätzel, M. *J. Phys. Chem. B* **2000**, *104*, 1300-1306.
(31) Greiner, M. T.; Helander, M. G.; Tang, W.-M.; Wang, Z.-B.; Qiu, J.; Lu, Z.-H. *Nat. mater.* **2012**, *11*, 76.
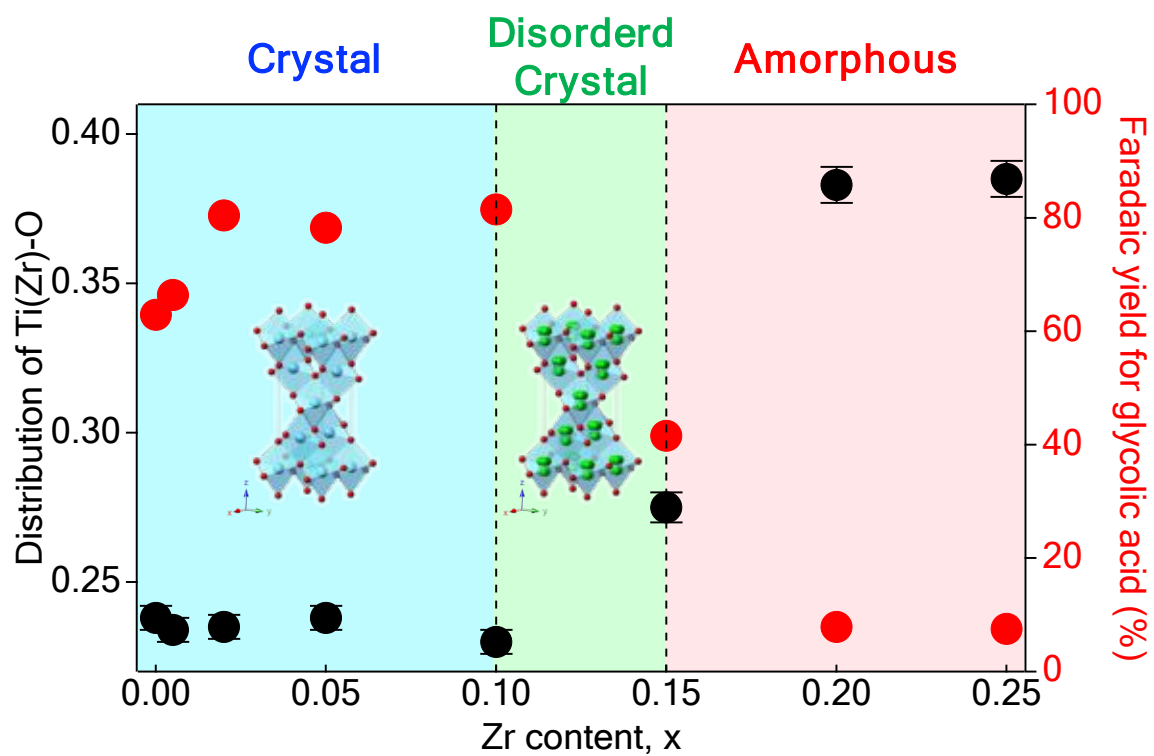
$Ti_{0.9}Zr_{0.1}O_2$ complex oxide particles exhibit superior catalytic performances for the direct power storage into glycolic acid via electroreduction of oxalic acid due to favorable crystallinity.